CreditDecoding: Accelerating Parallel Decoding in Diffusion Large Language Models with Trace Credits

Anonymous ACL submission

Abstract

Diffusion large language models (dLLMs) generate text through iterative denoising. In commonly adopted parallel decoding schemes, each step confirms only high-confidence positions while remasking the others. By analyzing dLLM denoising traces, we uncover a key inefficiency: models often predict the correct target token several steps before its confidence becomes high enough to be decoded. This gap between early prediction and late decoding forces repeated remasking of already-correct tokens, causing redundant iterations and limiting acceleration. To exploit this temporal redundancy, we introduce *Trace Credit* to quantify a token's decoding potential by accumulating historical evidence. Building on this, we propose **CreditDecoding**, a *training-free* parallel decoding method that fuses Trace Credit with current logits to boost the confidence of correct but underconfident tokens, thereby accelerating denoising and improving robustness. On eight benchmarks, CreditDecoding achieves up to 5.48× speedup with +0.48 accuracy on LLaDA-8B , and consistently improves performance across diverse dLLM architectures and parameter scales. It further scales to long contexts and remains orthogonal to mainstream inference optimizations, making it a practical and applicable solution.

1 Introduction

Diffusion-based large language models (dLLMs) have recently emerged as a promising alternative to autoregressive models (ARMs) for text generation (Ye et al., 2025; Nie et al., 2025; Zhu et al., 2025a,b; Gong et al., 2025b,a; Song et al., 2025; Yang et al., 2025; Kim et al., 2025a). Unlike ARMs that predict tokens strictly left-to-right, dLLMs generate text through iterative denoising with bidirectional attention, enabling richer contextual dependencies. This paradigm has demonstrated advantages in reasoning and generation quality (Nie et al., 2025; Ye et al., 2025). However, inference efficiency remains a major bottleneck: dLLMs typically require redundant denoising steps to predict all masked tokens, and the use of bidirectional attention precludes a lossless KV cache (Yu et al., 2025).

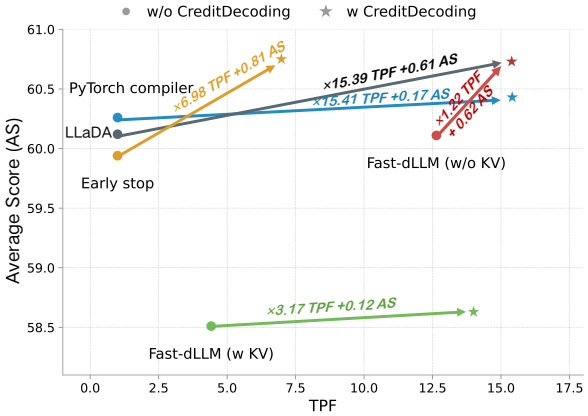

Figure 1: Acceleration methods (dots) vs. their performance with CreditDecoding (stars) on LLaDA.

To accelerate inference, recent work has focused on improving the effectiveness and efficiency of *parallel decoding* in dLLMs (Yu et al., 2025; Wei et al., 2025). At each denoising step, the model first predicts all masked tokens and then selects a subset of high-confidence positions to decode, while remasking the remaining uncertain tokens for future refinement (Yu et al., 2025). This strategy allows multiple tokens to be updated in parallel and has proven both simple and effective. Nevertheless, it suffers from two key limitations:

(i) Computational redundancy. In many cases, tokens are predicted early but decoded late due to low confidence, causing repeated prediction. Figure 5 shows the resulting temporal gap between initial prediction and final decoding.

(ii) History-agnostic Decoding. As the context is iteratively updated and may include mispredicted tokens, the confidence of otherwise stable tokens can fluctuate or even regress (Wang et al., 2025).

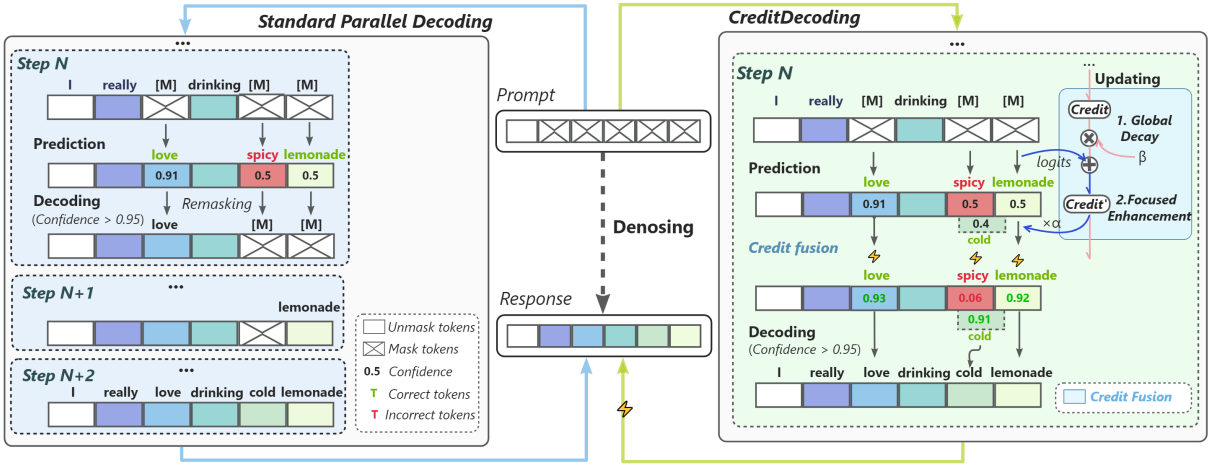

Figure 2: Comparison between **standard dLLM parallel decoding** (left) and the proposed **CreditDecoding** (right). The left diagram illustrates how existing methods predict solely on instantaneous predictions at each step, causing the repetitive remasking of correct tokens. In contrast, CreditDecoding maintains a token-level credit value across steps, using Trace Credit as a prior to enhance and calibrate current predictions.

However, token decoding is typically independent of predictions from previous steps, without leveraging the historical consistency of tokens. This undermines convergence and propagates errors across steps, reducing decoding robustness.

To address these issues, we propose **CreditDecoding**, a *training-free* parallel decoding strategy for dLLMs. It assigns each token a *trace credit score* that accumulates historical logits across steps. This score acts as a prior condition fused with the current logits to boost confidence. CreditDecoding reduces redundant iterations while stabilizing predictions against temporary inconsistencies.

We evaluate CreditDecoding on four dLLMs across eight benchmarks covering knowledge, reasoning, and coding. Experiments show that CreditDecoding achieves consistent speedups with modest performance uplift across a diverse set of dLLM architectures and benchmarks, while remaining orthogonal to mainstream optimizations such as KV cache (Feng et al., 2025) and kernel fusion (Jain et al., 2023). In summary, our work makes the following contributions:

- We analyze threshold-based parallel decoding and identify *computational redundancy* and *history-agnostic decisions* as key bottlenecks. We further find *temporal consistency* in confidence trajectories across denoising steps, providing an effective prior for acceleration.
- We propose **CreditDecoding**, a *training-free* method that accumulates trace credits as a token-level prior to accelerate inference. We also introduce a *tuning-free* variant to improve usability. On LLaDA-8B-Instruct, the primary approach achieves up to $5.48\times$ speedup while *improving* task performance.
- We demonstrate the *scalability*, *generality*, and *orthogonality* of CreditDecoding. It scales effectively across a wide range of model sizes and context lengths, while maintaining seamless compatibility with mainstream optimizations (Figure 1).

2 Related Work

Diffusion Language Models Diffusion large language models (dLLMs) replace left-to-right prediction with iterative denoising, enabling order-agnostic and parallel token updates with bidirectional context (Nie et al., 2025; Ye et al., 2025). Representative systems include Dream and the LLaDA family, with extensions to code, large-scale training, and multimodal/vision-conditioned settings (Ye et al., 2025; Nie et al., 2025; Zhu et al., 2025a,b; Gong et al., 2025b,a; Song et al., 2025; You et al., 2025; Yang et al., 2025). Variants further explore flexible-length and any-order masking (Kim et al., 2025a). Theoretically, dLLMs can approach autoregressive quality but typically require multiple denoising steps, with complexity that may grow with stricter sequence-level correctness and longer context (Feng et al., 2025; Liu et al., 2025a). Practically, unlike ARMs, dLLMs lack lossless KV caching and often incur high latency due to many denoising iterations (Cobbe et al., 2021; Hendrycks et al., 2021b; Chen et al., 2021; Jain et al., 2024).

Inference Acceleration and Decoding Strate-

gies To reduce latency, parallel decoding samples multiple tokens per step, and reuse or caching of bidirectional-attention outputs or other stable computations can further cut runtime without retraining (Yu et al., 2025; Wei et al., 2025; Liu et al., 2025b). Beyond speed, planning and ordering methods (e.g., path-planning remasking, adaptive ordering, calibration, or attention pruning) improve robustness and efficiency (Peng et al., 2025; Kim et al., 2025b; Huang et al., 2025; Chen et al., 2025), and some incorporate temporal/historical signals (Wang et al., 2025). However, many score-based strategies remain largely history-agnostic, relying on current-step confidence, which can induce step-level instability and redundant remasking until confidence converges.

3 Preliminary

3.1 Inference Process of dLLMs

A Diffusion Large Language Model (dLLMs) generates discrete text sequences by iteratively denoising a fully masked input. dLLMs formulate generation as a stochastic reverse denoising process that starts from an all-`[Mask]` sequence and gradually recovers the clean sequence.

Let $x \in \mathcal{V}^L$ be a sequence of length L over a vocabulary $\mathcal{V}$. At each discrete step $t \in \{0, \dots, T\}$, let x_t denote the corrupted sequence and $M_t \subseteq \{1, \dots, L\}$ be the set of masked positions. We use $\eta_t \in [0, 1]$ to denote the masked ratio, following a forward schedule where noise increases with t.

The core component is a denoising model f_θ that maps a corrupted sequence x_t to logits $l_t = f_\theta(x_t)$. These logits parameterize the probability distribution of the original token at each position i:

$$p_\theta^i(\cdot \mid x_t) = \mathrm{Softmax}(l_t^i). \tag{1}$$

This order-agnostic formulation enables the model to predict masked tokens based on arbitrary visible context. During inference, the denoising process starts from x_T and iteratively refines the state until the clean sequence x_0 is fully recovered. At each denoising step t, the transition from x_t to x_{t-1} is defined as:

$$x_{t-1} \sim \prod_{i=1}^{L} g_\theta(x_{t-1}^i \mid x_t), \tag{2}$$

where the transition kernel g_θ is given by:

$$g_\theta(x_{t-1}^i \mid x_t) = \begin{cases} x_t^i, & i \notin M_t, \\ \mathrm{Cat}(\pi_t^i), & i \in M_t. \end{cases} \tag{3}$$

Here, $\pi_t^i(\cdot) = \frac{\eta_{t-1}}{\eta_t}\mathbf{e}_M + \frac{\eta_t - \eta_{t-1}}{\eta_t} p_\theta^i(\cdot \mid x_t)$, and $\mathbf{e}_M$ denotes the one-hot vector of the `[Mask]`.

Intuitively, at each masked position, the token either remains masked or is predicted by the model based on the schedule. In practical parallel decoding, high-confidence tokens from $p_\theta(\cdot|x_t)$ are decoded and updated into x_{t-1}, while uncertain positions are remasked for future refinement. This procedure iterates until $M_0 = \varnothing$.

Moreover, many implementations adopt a **block-wise** strategy: the sequence is partitioned into blocks, and tokens within the current block can be decoded while external tokens serve as fixed context. This limits the impact of uncertain tokens, reducing error propagation and improving stability.

3.2 Parallel Decoding

dLLMs naturally support recovering mask tokens in parallel. Assuming conditional independence at each step t, the joint distribution is approximated by the product of marginals. For each masked position $i \in M_t$ and token $v \in \mathcal{V}$, we **greedily sample** candidate tokens $\tilde{x}_t^i = \arg\max_v p_\theta^i(v \mid x_t)$ and its confidence score $s_t^i = p_\theta^i(\tilde{x}_t^i \mid x_t)$.

Previous work validates that high-confidence marginals effectively approximate the joint distribution (Wu et al., 2025). Based on this, the mainstream strategy decodes a subset of tokens $I_t = \{i \in M_t \mid s_t^i \geq \tau\}$ whose confidence exceeds a threshold τ. Tokens in I_t are decoded in parallel, while the rest remain masked (Figure 2).

Beyond simple probability, other scoring functions (e.g., negative entropy, probability margins.) and sampling schemes (e.g., top-k, adaptive schedules) have also been explored.

4 Methodology

4.1 Observations

In this section, we analyze limitations of threshold-based parallel decoding in dLLM inference. For each position i, we define the ***target token*** $x_0^{i,v}$ as the token with ID v ultimately decoded at position i in the final output sequence.

Figure 3 (blue line) visualizes how the confidence of $x_0^{i,v}$ evolves over denoising process. Many tokens are repeatedly sampled as candidate tokens and predicted long before they get final decoded. particularly pronounced under single-token decoding schemes, which, despite this inefficiency, often lead to higher final accuracy (Feng et al., 2025).

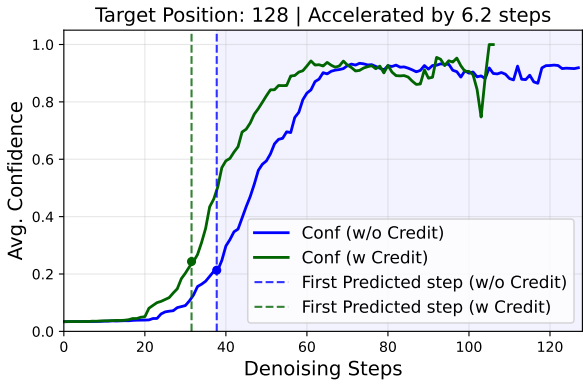

Figure 3: Impact of CreditDecoding on $x_0^{128,v}$ confidence. The shadow region marks steps where $x_0^{128,v}$ achieves top-1 conf, CreditDecoding reduces steps by boosting confidence and entering this region earlier.

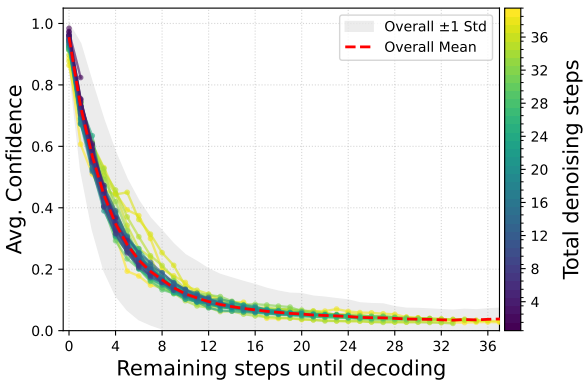

Figure 4: Temporal consistency. Results are obtained on GSM8K with threshold-based parallel decoding. Curves correspond to tokens grouped by total denoising steps.

This observation reveals two limitations of existing methods: **(i) Redundant computation.** Decisions are gated by instantaneous confidence, so correct hypotheses are repeatedly predicted and remasked until s_t^i exceeds τ. **(ii) History-agnostic decoding.** Each step ignores past predictions; transient mispredictions can delay decoding and propagate errors to later denoising steps.

A natural idea is to *promote early decoding* by boosting the confidence of target tokens so that they cross the threshold earlier. For practicality and analytical tractability in the probability domain, we add a gain of the form $\log X$ ($X \geq 1$) to the target-token logit. Specifically, for a target token $x_0^{i,v}$, we enhance its logit $l_t^{i,v}$ as:

$$\hat{l}_t^{i,v} = l_t^{i,v} + \log X, \tag{4}$$

where $\hat{l}_t^{i,v}$ is the corresponding fused logit.

Let $p_t^{i,v} = p_\theta^i(v \mid x_t)$ denote the current probability of token v at position i. When $x_0^{i,v}$ is the predicted token at step t, we have $s_t^i = p_t^{i,v}$. It is straightforward to show that the *minimum* gain required to ensure $\hat{s}_t^i = \hat{p}_t^{i,v} \geq \tau$ is:

$$X \;\geq\; X_{\min}(p_t^{i,v}, \tau) = \frac{\tau}{1-\tau} \cdot \left(\frac{1}{p_t^{i,v}} - 1\right). \tag{5}$$

Eq. 5 shows that the required gain is highly sensitive to $\hat{p}_t^{i,v}$. However, early-step probabilities are unstable and the true target token is unknown. Naively applying $X_{\min}$ can amplify noise and lead to irreversible decoding errors. This motivates a token-level **trace credit** $C_t^{i,v}$ that aggregates historical evidence and serves as an adaptive gain for the current prediction. Intuitively, credit measures a candidate's likelihood of converging to high confidence, enabling earlier yet safer decoding. The derivation is provided in Appendix C.1.

4.2 CreditDecoding

In this section, we introduce *CreditDecoding*, a training-free mechanism that enables earlier and safer decoding in parallel decoding.

Temporal Consistency Formally, we define the denoising trace $\mathcal{T}$ as the ordered collection of predicted tokens and their confidence during the denoising process. Specifically, at each step t from T down to 0, all predicted tokens $\tilde{x}_t$ and confidence scores s_t are appended to $\mathcal{T}$.

As shown in Figure 4, the confidence of the eventual target token $x_0^{i,v}$ exhibits a consistently increasing trend and quickly approaches 1 as it nears decoding. Moreover, this trend is largely insensitive to the length of $\mathcal{T}$, suggesting that the confidence of a target token is determined mainly by its *denoising stage* (i.e., the remaining steps).

Motivated by this property, we use an EMA-based credit to aggregate temporal evidence into a stable prior, predicting whether the current greedy token $\tilde{x}_t^i$ will eventually be decoded.

Definition of Trace Credit During inference, we maintain token-level credits independently for each position. At each denoising step t, for every masked position $i \in M_t$ and token $v \in \mathcal{V}$, we maintain a credit value $C_t^{i,v} \in \mathbb{R}_{\geq 0}$ that accumulates historical evidence from $\mathcal{T}$ for supporting token v at position i. Given the predicted token $\tilde{x}_t^i$, credits are updated via an EMA-style rule that reinforces $\tilde{x}_t^i$:

$$C_t^{i,v} = \begin{cases} \beta\, C_{t+1}^{i,v} + \left(p_t^{i,v}\right)^\gamma, & v = \tilde{x}_t^i, \\ \beta\, C_{t+1}^{i,v}, & \text{otherwise.} \end{cases} \tag{6}$$

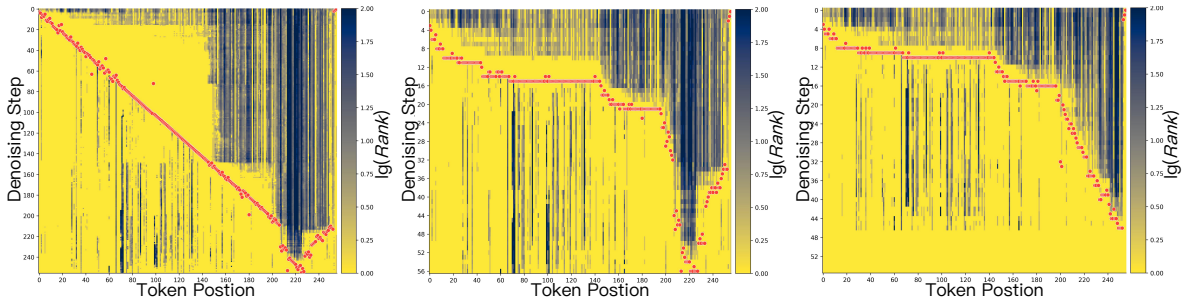

Figure 5: Confidence rank of the target token $x_0^{i,v}$(defined in 4.1) at each position i during the generation steps s (**Left**: LLaDA, **Middle**: Fast-dLLM, **Right**: CreditDecoding). The red dots denote that the model decodes token at pos i at the corresponding step s, which is also the *Decoding Boundary* in FigureC.3.

Here $\beta \in (0, 1)$ controls exponential decay, and $\gamma \in (0, 1)$ is a concave transform that up-weights low-confidence values, which is fixed in our implementation.

As illustrated in Figure 2, this update rule balances two dynamics. **(i) Global decay**: β gradually forgets stale evidence, especially from tokens not currently predicted, suppressing early-stage confidence fluctuations. **(ii) Focused enhancement**: only the currently predicted token $\tilde{x}_t^i$ receives an additional credit boost, so credit accumulates mainly on tokens that remain consistently top-1 along the denoising trace rather than on transient spikes.

For completeness, we also explore a variant that aggregates historical evidence for all tokens. Details are given in Appendix C.8.

Crucially, we fuse credit with logits to obtain a sharpened predictive distribution:

$$\hat{l}_t^{i,v} = l_t^{i,v} + \alpha \cdot \log\big(C_t^{i,v} + 1\big) \tag{7}$$

where $\alpha > 0$ controls the strength of the credit-based prior. Eq. 7 is equivalent to applying a multiplicative gain to $p_t^{i,v}$ in the probability domain, yielding $\hat{p}_t^{i,\cdot} = \mathrm{Softmax}\big(\hat{l}_t^i\big)$.

Accordingly, the confidence score becomes $\hat{s}_t^i = \max_{v \in \mathcal{V}} \hat{p}_t^{i,v}$, and the predicted token under the enhanced distribution is $\tilde{x}_t^i = \arg\max_v \hat{p}_t^{i,v}$. Tokens predicted consistently across steps thus accumulate credit, inducing an growing effective gain that enables earlier decoding and reduces redundant remasking. Conversely, unstable candidates are down-weighted by decay, improving robustness to transient fluctuations. In practice, we apply CreditDecoding only within the *current denoising block* for inference efficiency. Algorithm 1 provides the complete procedure.

Importantly, CreditDecoding modifies only the output logits and seamlessly integrates with mainstream inference optimizations to achieve cumulative speedups.

4.3 Tuning-Free Schedule

To avoid hyperparameter tuning, we propose a step-adaptive schedule that couples credit strength to the denoising stage.

Let η_t denote the mask ratio at step t. We set $\gamma = 1$ and use step-dependent coefficients $\beta_t = \alpha_t = 1 - \eta_t$ to reflect the denoising progress, where α_t is the logit-fusion weight in Eq. 7.

In early steps, it down-weights trace credits to counter unreliable confidence. As denoising progresses and η_t decreases, predictions stabilize and credit strength increases automatically.

5 Experiments

5.1 Experimental Setup

Implementation We implement CreditDecoding on LLaDA-8B-Instruct (Nie et al., 2025) and LLaDA-MoE-Instruct (Zhu et al., 2025b). Inference settings differ across experiments and may deviate slightly from from the original papers. We detail them in the corresponding sections. All experiments are conducted on NVIDIA H20-3e 140 GB GPUs.

In the main experiments, we set the generation length and number of steps to 256. Additional experiments with different generation lengths are reported in Section 5.5. Based on the analyses in Appendix C.4 and Section 5.3, we set the block size to 64, and the hyperparameters of CreditDecoding to $\alpha = 0.65$, $\beta = 0.7$ and $\gamma = 0.2$.

Evaluation Tasks In the main experiments, we comprehensively evaluate CreditDecoding on eight datasets spanning five categories. Specifically, we evaluate inference performance on DROP (Dua et al., 2019) and KorBench (Ma et al., 2025a),

Table 1: Main benchmark results **w/ Early Stop** across eight datasets on LLaDA-8B-Instruct and LLaDA-MoE-Instruct(Gen Length=256, Block Size=64 . Cells show **Score** (top, relative to LLaDA) and **TPF** (bottom, improvement over Fast-dLLM). The last row (**Avg.**) reports the mean Score and mean TPF over the eight datasets.

Benchmark	LLaDA-8B-Instruct			LLaDA-MoE-Instruct		
	Baseline	Fast-dLLM	CreditDecoding	Baseline	Fast-dLLM	CreditDecoding
MMLU $^{SCORE}_{TPF}$	62.46 1	62.43 $_{-0.03}$ 2.86	**63.78** $_{+1.32}$ **4.57** (*+56%*)	64.08 1	64.08 $_{0.00}$ 2.16	**64.21** $_{+0.13}$ **2.46** (*+14%*)
SQuAD2.0 $^{SCORE}_{TPF}$	91.43 1	91.43 $_{0.00}$ 13.55	**91.71** $_{+0.28}$ **16.84** (*+24%*)	86.88 1	86.88 $_{0.00}$ 7.09	**87.27** $_{+0.39}$ **9.64** (*+36%*)
DROP $^{SCORE}_{TPF}$	82.86 1	82.74 $_{-0.12}$ 2.93	**82.78** $_{-0.08}$ **3.79** (*+29%*)	**80.16** 1	**80.16** $_{0.00}$ 2.73	79.72 $_{-0.44}$ **3.28** (*+20%*)
KorBench $^{SCORE}_{TPF}$	33.12 1	33.20 $_{+0.08}$ 3.72	**35.04** $_{+1.92}$ **5.03** (*+35%*)	36.72 1	**36.88** $_{+0.16}$ 2.36	36.48 $_{-0.24}$ **3.28** (*+38%*)
HumanEval $^{SCORE}_{TPF}$	34.76 1	34.15 $_{-0.61}$ 3.82	**36.59** $_{+1.83}$ **4.69** (*+23%*)	**51.22** 1	**51.22** $_{0.00}$ 4.97	**51.22** $_{0.00}$ **6.00** (*+21%*)
LCB $^{SCORE}_{TPF}$	**8.15** 1	**8.15** $_{0.00}$ 1.93	7.54 $_{-0.61}$ **2.17** (*+12%*)	13.88 1	14.04 $_{+0.16}$ 2.43	**14.37** $_{+0.49}$ **2.81** (*+16%*)
GSM8K $^{SCORE}_{TPF}$	77.94 1	**78.47** $_{+0.53}$ 3.22	77.18 $_{-0.76}$ **3.87** (*+20%*)	74.37 1	74.45 $_{+0.08}$ 2.28	**74.98** $_{+0.61}$ **2.68** (*+18%*)
Math $^{SCORE}_{TPF}$	37.30 1	37.04 $_{-0.26}$ 2.42	**37.24** $_{-0.06}$ **2.84** (*+17%*)	36.02 1	35.84 $_{-0.18}$ 2.35	**36.28** $_{+0.26}$ **2.71** (*+15%*)
Average $^{SCORE}_{TPF}$	53.50 1	53.45 $_{-0.05}$ 4.31	**53.98** $_{+0.48}$ **5.48** (*+27%*)	55.42 1	55.44 $_{+0.02}$ 3.30	**55.57** $_{+0.15}$ **4.11** (*+25%*)

language understanding on SQuAD, knowledge assessment on MMLU (Hendrycks et al., 2021a), coding ability on OpenAI HumanEval (Chen et al., 2021) and LiveCodeBench (Jain et al., 2024), and mathematical reasoning on GSM8K (Cobbe et al., 2021) and Math (Hendrycks et al., 2021b). In the ablation, scaling, and other analysis experiments, due to computational constraints, we select five representative datasets across categories: MMLU, SQuAD, KorBench, HumanEval, and GSM8K.

Evaluation metric We adopt the standard performance metrics for each evaluation dataset, as detailed in Appendix B. In addition, to examine whether CreditDecoding can mitigate redundant computation inherent in traditional dLLMs, we utilize *TPF* (Tokens Per Forward) to evaluate dLLM inference efficiency. We report single-run results for each setting.

Early Stop In dLLM, early stopping changes the generated length and thus significantly affects TPF. Some studies disable it to boost TPF, as the model quickly outputs the EOS token. However, in practical applications it is usually enabled to avoid redundant outputs. We *enable* Early Stop by default, except in Figure 1 for better comparison.

5.2 Main Results

As shown in Table 1, we evaluate our method on eight datasets using LLaDA-8B-Instruct and LLaDA-MoE-Instruct. We use each benchmark's default performance metric and report TPF for inference speed, with TPF of the baseline normalized to 1. TPF of CreditDecoding thus directly reflects speedup relative to the baseline.

Overall, ***CreditDecoding outperform the baseline and SOTA Fast-dLLM in both performance and speed***. It achieves a 5.48× speedup and 0.48 performance gain on LLaDA-8B-Instruct, and a 4.10× speedup on LLaDA-MoE-Instruct.

Figure 5 illustrates that after applying CreditDecoding, the red line representing the step of decoding each token prediction becomes more horizontal, indicating more parallel decoding within each step and higher efficiency. While the baseline requires all 256 steps, CreditDecoding completes decoding in 50 steps, consistent with the 5× speedup in

Table 2: Performance comparison across different model paradigms and scales. Results are reported as the average **Score / TPF** over the evaluated datasets. CD refers to CreditDecoding.

Paradigm	Arch.	Model	Params	Fast-dLLM	CD	CD-Adaptive
Pure Diffusion	Dense	LLaDA	8B	60.38 / 5.49	**60.86** / 7.00	60.23 / **7.74**
	MoE	LLaDA-MoE	7B-A1B	62.70 / 3.77	62.83 / 4.81	**63.74** / **5.27**
Block Diffusion	MoE	LLaDA2-Mini	16B-A1B	76.23 / 2.01	76.69 / **2.26**	**76.92** / 2.15
	MoE	LLaDA2-Flash	100B-A6B	84.89 / 2.48	84.53 / **2.79**	**84.97** / 2.68

Table 1. Yellow and blue denote high and low confidence respectively, with their boundary marking the step where the model predict the target token for the first time. The gap between the red line and the boundary shows the redundant steps the decoding method brings. Traditional dLLMs discard remasked token information, necessitating repeated predictions and creating a gap between the red line and the yellow-blue boundary.

Two observations in Figure 5 explain why CreditDecoding speeds up decoding: The yellow-blue boundary moves upward, denoting that model predict the target token earlier, improving the upper limit of the red line. CreditDecoding decreases the gap between the red line and the yellow-blue boundary which mitigate redundant steps.

5.3 Hyperparameter Ablation Study

As discussed in Section 4.2, CreditDecoding has three hyperparameters: β for global decay, α for logits fusion, and γ for concave amplification. We fix γ and perform ablation studies on α and β in the range [0, 0.95] with a step size of 0.05.

Figure 6 shows that performance fluctuates slightly with α and β, peaking around $\beta = 0.5$ and $\beta = 0.7$, while α remains stable within [0.2, 0.65]. ***Larger values of both parameters increase TPF by accumulating more trace credit, but may reduce accuracy.*** We select $\alpha = 0.65$ and $\beta = 0.7$ as they provide a good trade-off, yielding strong performance and high TPF across five datasets, though optimal values vary by dataset.

5.4 Generalizability

In this section, we demonstrate the generalizability of CreditDecoding by conducting experiments across models characterized by diverse paradigms and scales. As shown in Table 2, in addition to the LLaDA-8B-Ins and LLaDA-MoE-Ins models discussed in the main results, we extended our evaluation to include LLaDA2-Mini and LLaDA2-Flash(Bie et al., 2025). Collectively, these experiments encompass various training paradigms and

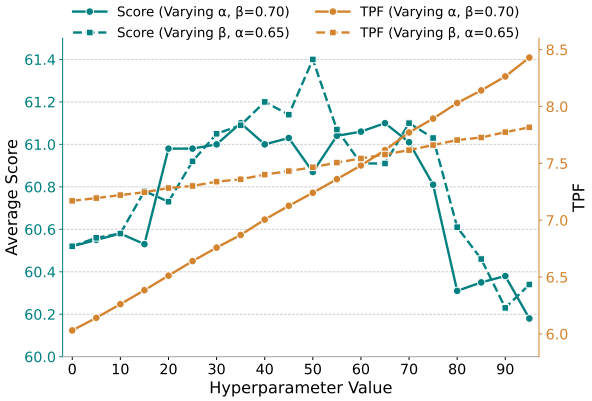

Figure 6: Hyperparameter Ablation. Green: average score; Yellow: average TPF. **Solid**: varying α with fixed $\beta = 0.70$; **Dashed**: varying β with fixed $\alpha = 0.65$.

architectures, spanning parameter scales from 8B to 100B. We employed dInfer (Ma et al., 2025b) for inference on LLaDA2-Mini and LLaDA2-Flash, configuring the generation length to 2048 and the block size to 32. Due to computational constraints, we limit our comparison to Fast-dLLM, CreditDecoding, and the CreditDecoding-Adaptive, which adapts to the step mask ratio introduced in Section 4.3, omitting weaker baselines that are incompatible with parallel decoding.

Results in Table 2 yield two critical insights. First, ***CreditDecoding strategy delivers more substantial efficiency gains in Pure Diffusion training paradigms*** due to its larger attention context window. Second, and most significantly, ***CreditDecoding-Adaptive serves as a universal, tuning-free solution***. Addressing the dataset-dependent nature of denoising traces $\mathcal{T}$ (Appendix C.6), it eliminates the need for task-specific hyperparameter tuning, thereby reducing deployment overhead. It yields superior generation scores and remains significantly faster than Fast-dLLM, balancing performance and usability with minimal efficiency cost.

5.5 Scalability

Current research on dLLMs typically evaluates generation lengths of 128 or 256, with a few studies

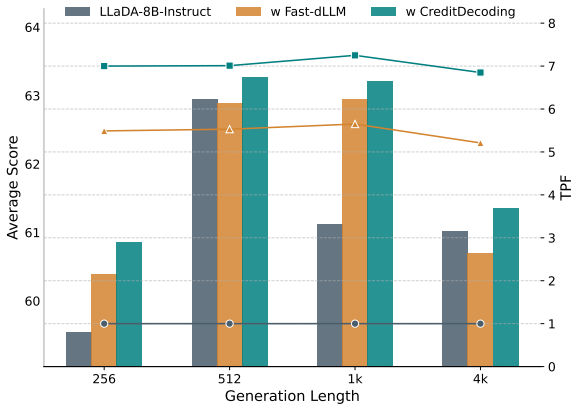

Figure 7: Scalability of CreditDecoding on LLaDA. Lines indicate average TPF; bars show average score.

extending to 512. However, the primary advantage of dLLMs over autoregressive models—parallel decoding—is largely underutilized at such short lengths. To address this, in this section we scale the generation length to 1024 and 4096, aiming to provide insights into the potential of dLLMs for long-text generation.

We fix the number of steps equal to the generation length and set the block size to 64. Figure 7 shows that both the baseline and CreditDecoding peak at length 512 and gradually degrade as length increases. Notably, ***CreditDecoding consistently outperforms the baseline and scales better with generation length***, demonstrating stronger robustness in long-context scenarios

Crucially, the method sustains a consistent $7\times$ TPF speedup across settings. As text length grows, ***this relative speedup translates into increasingly substantial absolute latency reductions***, highlighting its practical value in long-context scenarios.

5.6 Orthogonality

CreditDecoding operates purely on the model logits and does not interfere with the *sample* or *select* procedures. This design makes it a ***plug-and-play*** post-processing module that is naturally orthogonal to both (i) system-level inference optimizations such as compiler-level acceleration (Jain et al., 2023), and (ii) algorithmic acceleration strategies for dLLMs such as threshold decoding, KV-cache variants, and EOS early stopping.

In all cases, we keep the hyperparameters and selection rules of the baseline methods unchanged, and only apply CreditDecoding on top. As demonstrated in Figure 1, our experiments confirm this orthogonality. When combined with CreditDecoding, we observe that the speedup is preserved while the performance drop is partially mitigated, showing that historical trace credit acts as a stabilizing prior under aggressive compression.

For algorithmic acceleration, threshold parallel decoding (Fast-dLLM w/o KV cache (Wu et al., 2025)) typically accelerates but at the cost of lower accuracy. For EOS early stopping, CreditDecoding complements the strategy by improving robustness of token selection in earlier steps. Adding CreditDecoding further boosts both speed and accuracy, with $4.7\times$ acceleration over the baseline with an additional $+0.63$ improvement in average score. Similarly, CreditDecoding alleviates the accuracy loss of threshold decoding and complements KV-cache methods by reducing redundant iterations within cached segments. These results above demonstrate that ***CreditDecoding can be seamlessly integrated with existing optimizations to deliver consistent performance gains***.

Appendix C.7 provides details of our acceleration methods and orthogonality experimental results for CreditDecoding on LLaDA and LLaVA-MoE, including **inference throughput (TPS)**.

6 Conclusion

The history-agnostic decoding process of diffusion language models inherently suffers from substantial computational redundancy. To address this, we propose CreditDecoding, a training-free decoding strategy orthogonal to mainstream acceleration methods. Specifically, it assigns a trace credit to each candidate token by accumulating historical logit predictions from remasked steps, and subsequently fuses this credit into the current logits.

By fully leveraging the model's past predictions on remasked tokens for the first time, CreditDecoding reduces the complexity of current inference steps. This leads to simultaneous improvements in performance and decoding efficiency, achieving a $5.48\times$speedup and an average accuracy gain of $+0.48$ compared to standard LLaDA-8B-Instruct.

Ultimately, CreditDecoding aims to approach the theoretical limit of acceleration (indicated by the yellow-blue boundary in Figure 5). As more powerful base models emerge, the acceleration ceiling of CreditDecoding will rise, leading to further efficiency gains in model inference.

Limitations

Although CreditDecoding provides consistent acceleration and accuracy gains, it also has several limitations.

First, it relies on the accumulation of historical evidence along the denoising trace, and thus requires a certain number of denoising steps to build effective trace credit. For pure-diffusion dLLMs that adopt small block sizes to sacrifice inference efficiency in exchange for better performance, and for dLLMs that are explicitly trained for aggressive parallel decoding whose logit distributions are sharp with fast confidence convergence, our approach may not have enough denoising steps to accumulate sufficient trace credit. In these cases, the acceleration benefit becomes limited. Experiments in the Appendix C.4 also show that increasing the block size generally allows stronger credit accumulation and leads to larger speedup.

Second, due to variations in dataset characteristics, such as data pattern or sample difficulty, and inherent model behavior, the optimal setting for α, β and γ may differ across tasks and models. Although we propose a tuning-free adaptive variant in Sec. 4.3 that yields stable and consistent improvements across model architectures, benchmarks, and parameter scales, it does not always achieve the theoretically optimal performance–efficiency trade-off. In practice, obtaining best benefit still requires lightweight hyperparameter search on a small validation set.

References

Tiwei Bie, Maosong Cao, Kun Chen, Lun Du, Mingliang Gong, Zhuochen Gong, Yanmei Gu, Jiaqi Hu, Zenan Huang, Zhenzhong Lan, and 1 others. 2025. Llada2. 0: Scaling up diffusion language models to 100b. *arXiv preprint arXiv:2512.15745*.

Mark Chen, Jerry Tworek, Heewoo Jun, Qiming Yuan, Henrique Ponde de Oliveira Pinto, Jared Kaplan, Harri Edwards, Yuri Burda, Nicholas Joseph, Greg Brockman, Alex Ray, Raul Puri, Gretchen Krueger, Michael Petrov, Heidy Khlaaf, Girish Sastry, Pamela Mishkin, Brooke Chan, Scott Gray, and 39 others. 2021. Evaluating large language models trained on code. *Preprint*, arXiv:2107.03374.

Xinhua Chen, Sitao Huang, Cong Guo, Chiyue Wei, Yintao He, Jianyi Zhang, Hai "Helen" Li, and Yiran Chen. 2025. Dpad: Efficient diffusion language models with suffix dropout. *Preprint*, arXiv:2508.14148.

Karl Cobbe, Vineet Kosaraju, Mohammad Bavarian, Mark Chen, Heewoo Jun, Lukasz Kaiser, Matthias Plappert, Jerry Tworek, Jacob Hilton, Reiichiro Nakano, Christopher Hesse, and John Schulman. 2021. Training verifiers to solve math word problems. *Preprint*, arXiv:2110.14168.

Dheeru Dua, Yizhong Wang, Pradeep Dasigi, Gabriel Stanovsky, Sameer Singh, and Matt Gardner. 2019. Drop: A reading comprehension benchmark requiring discrete reasoning over paragraphs. *Preprint*, arXiv:1903.00161.

Guhao Feng, Yihan Geng, Jian Guan, Wei Wu, Liwei Wang, and Di He. 2025. Theoretical benefit and limitation of diffusion language model. *Preprint*, arXiv:2502.09622.

Shansan Gong, Shivam Agarwal, Yizhe Zhang, Jiacheng Ye, Lin Zheng, Mukai Li, Chenxin An, Peilin Zhao, Wei Bi, Jiawei Han, Hao Peng, and Lingpeng Kong. 2025a. Scaling diffusion language models via adaptation from autoregressive models. *Preprint*, arXiv:2410.17891.

Shansan Gong, Ruixiang Zhang, Huangjie Zheng, Jiatao Gu, Navdeep Jaitly, Lingpeng Kong, and Yizhe Zhang. 2025b. Diffucoder: Understanding and improving masked diffusion models for code generation. *Preprint*, arXiv:2506.20639.

Dan Hendrycks, Collin Burns, Steven Basart, Andy Zou, Mantas Mazeika, Dawn Song, and Jacob Steinhardt. 2021a. Measuring massive multitask language understanding. *Preprint*, arXiv:2009.03300.

Dan Hendrycks, Collin Burns, Saurav Kadavath, Akul Arora, Steven Basart, Eric Tang, Dawn Song, and Jacob Steinhardt. 2021b. Measuring mathematical problem solving with the math dataset. *Preprint*, arXiv:2103.03874.

Pengcheng Huang, Shuhao Liu, Zhenghao Liu, Yukun Yan, Shuo Wang, Zulong Chen, and Tong Xiao. 2025. Pc-sampler: Position-aware calibration of decoding bias in masked diffusion models. *Preprint*, arXiv:2508.13021.

Animesh Jain, Shunting Zhang, Edward Yang, and 1 others. 2023. Pytorch 2.0: Our next generation 2.0 release.

Naman Jain, King Han, Alex Gu, Wen-Ding Li, Fanjia Yan, Tianjun Zhang, Sida Wang, Armando Solar-Lezama, Koushik Sen, and Ion Stoica. 2024. Livecodebench: Holistic and contamination free evaluation of large language models for code. *Preprint*, arXiv:2403.07974.

Jaeyeon Kim, Lee Cheuk-Kit, Carles Domingo-Enrich, Yilun Du, Sham Kakade, Timothy Ngotiaoco, Sitan Chen, and Michael Albergo. 2025a. Any-order flexible length masked diffusion. *Preprint*, arXiv:2509.01025.

Jaeyeon Kim, Kulin Shah, Vasilis Kontonis, Sham Kakade, and Sitan Chen. 2025b. Train for the worst, plan for the best: Understanding token ordering in masked diffusions. *Preprint*, arXiv:2502.06768.

Woosuk Kwon, Zhuohan Li, Siyuan Zhuang, Ying Sheng, Lianmin Zheng, Cody Hao Yu, Joseph E. Gonzalez, Hao Zhang, and Ion Stoica. 2023. Efficient memory management for large language model serving with pagedattention. *Preprint*, arXiv:2309.06180.

Xiaoran Liu, Zhigeng Liu, Zengfeng Huang, Qipeng Guo, Ziwei He, and Xipeng Qiu. 2025a. Longllada: Unlocking long context capabilities in diffusion llms. *Preprint*, arXiv:2506.14429.

Zhiyuan Liu, Yicun Yang, Yaojie Zhang, Junjie Chen, Chang Zou, Qingyuan Wei, Shaobo Wang, and Linfeng Zhang. 2025b. dllm-cache: Accelerating diffusion large language models with adaptive caching. *Preprint*, arXiv:2506.06295.

Kaijing Ma, Xinrun Du, Yunran Wang, Haoran Zhang, Zhoufutu Wen, Xingwei Qu, Jian Yang, Jiaheng Liu, Minghao Liu, Xiang Yue, Wenhao Huang, and Ge Zhang. 2025a. Kor-bench: Benchmarking language models on knowledge-orthogonal reasoning tasks. *Preprint*, arXiv:2410.06526.

Yuxin Ma, Lun Du, Lanning Wei, Kun Chen, Qian Xu, Kangyu Wang, Guofeng Feng, Guoshan Lu, Lin Liu, Xiaojing Qi, and 1 others. 2025b. dinfer: An efficient inference framework for diffusion language models. *arXiv preprint arXiv:2510.08666*.

Shen Nie, Fengqi Zhu, Zebin You, Xiaolu Zhang, Jingyang Ou, Jun Hu, Jun Zhou, Yankai Lin, Ji-Rong Wen, and Chongxuan Li. 2025. Large language diffusion models.

Fred Zhangzhi Peng, Zachary Bezemek, Sawan Patel, Jarrid Rector-Brooks, Sherwood Yao, Avishek Joey Bose, Alexander Tong, and Pranam Chatterjee. 2025. Path planning for masked diffusion model sampling. *Preprint*, arXiv:2502.03540.

Yuxuan Song, Zheng Zhang, Cheng Luo, Pengyang Gao, Fan Xia, Hao Luo, Zheng Li, Yuehang Yang, Hongli Yu, Xingwei Qu, Yuwei Fu, Jing Su, Ge Zhang, Wenhao Huang, Mingxuan Wang, Lin Yan, Xiaoying Jia, Jingjing Liu, Wei-Ying Ma, and 3 others. 2025. Seed diffusion: A large-scale diffusion language model with high-speed inference. *Preprint*, arXiv:2508.02193.

Wen Wang, Bozhen Fang, Chenchen Jing, Yongliang Shen, Yangyi Shen, Qiuyu Wang, Hao Ouyang, Hao Chen, and Chunhua Shen. 2025. Time is a feature: Exploiting temporal dynamics in diffusion language models. *Preprint*, arXiv:2508.09138.

Qingyan Wei, Yaojie Zhang, Zhiyuan Liu, Dongrui Liu, and Linfeng Zhang. 2025. Accelerating diffusion large language models with slowfast sampling: The three golden principles. *Preprint*, arXiv:2506.10848.

Chengyue Wu, Hao Zhang, Shuchen Xue, Zhijian Liu, Shizhe Diao, Ligeng Zhu, Ping Luo, Song Han, and Enze Xie. 2025. Fast-dllm: Training-free acceleration of diffusion llm by enabling kv cache and parallel decoding. *Preprint*, arXiv:2505.22618.

Ling Yang, Ye Tian, Bowen Li, Xinchen Zhang, Ke Shen, Yunhai Tong, and Mengdi Wang. 2025. Mmada: Multimodal large diffusion language models. *Preprint*, arXiv:2505.15809.

Jiacheng Ye, Zhihui Xie, Lin Zheng, Jiahui Gao, Zirui Wu, Xin Jiang, Zhenguo Li, and Lingpeng Kong. 2025. Dream 7b: Diffusion large language models.

Zebin You, Shen Nie, Xiaolu Zhang, Jun Hu, Jun Zhou, Zhiwu Lu, Ji-Rong Wen, and Chongxuan Li. 2025. Llada-v: Large language diffusion models with visual instruction tuning. *Preprint*, arXiv:2505.16933.

Runpeng Yu, Xinyin Ma, and Xinchao Wang. 2025. Dimple: Discrete diffusion multimodal large language model with parallel decoding. *Preprint*, arXiv:2505.16990.

Fengqi Zhu, Rongzhen Wang, Shen Nie, Xiaolu Zhang, Chunwei Wu, Jun Hu, Jun Zhou, Jianfei Chen, Yankai Lin, Ji-Rong Wen, and 1 others. 2025a. Llada 1.5: Variance-reduced preference optimization for large language diffusion models.

Fengqi Zhu, Zebin You, Yipeng Xing, Zenan Huang, Lin Liu, Yihong Zhuang, Guoshan Lu, Kangyu Wang, Xudong Wang, Lanning Wei, Hongrui Guo, Jiaqi Hu, Wentao Ye, Tieyuan Chen, Chenchen Li, Chengfu Tang, Haibo Feng, Jun Hu, Jun Zhou, and 7 others. 2025b. Llada-moe: A sparse moe diffusion language model. *Preprint*, arXiv:2509.24389.

A Statements

In this section, we provide clarifications on issues that require explicit statements. The Ethics Statement is omitted, as this work does not raise any ethical concerns.

A.1 Reproducibility.

We employed four widely adopted and advanced dLLM models, LLaDA-8B-Instruct, LLaDA-MoE-Instruct, LLaDA2-Mini and LLaDA2-Flash, along with their publicly available weights. Detailed experimental configurations for each setup are provided, and the specific metric configurations for score evaluation are included in Appendix B. We utilized TPF, a metric that is relatively robust to confounding factors, as it is not influenced by the number of GPUs, hardware model, or inference framework. Therefore, we argue that the results reported in this paper are highly reproducible.

A.2 Use of LLMs

In this study, LLMs were used solely to enhance the accuracy, coherence, and academic quality of the writing. We ensure that we did not use LLMs to generate any data or substantive content. All data are derived from our experiments, and all analyses and conclusions are the authors' own. LLMs were employed only to improve readability and facilitate readers' understanding of our experiments and findings.

B Evaluation Config

Table 3: Benchmarks, their corresponding evaluation metrics, and In-Context Learning (ICL) setup.

Benchmark	Metric	ICL
GSM8K	Accuracy	0-shot
Math	Accuracy	0-shot
SQuAD2.0	Score	1-shot
DROP	Score	2-shot
MMLU	Weighted Average	0-shot
KorBench	Naive Average	0-shot
LCB OC Code Generation v6	Score	0-shot
OpenAI HumanEval	Pass@1	0-shot

We employed OpenCompass to assist in the evaluation process, ensuring a standardized and systematic assessment. For each benchmark(LCB for LiveCodeBench), we utilized the specific metrics presented in Table 3, which allowed for a consistent and comprehensive comparison across different tasks. Regarding in-context learning (ICL) configurations, all benchmarks were evaluated in a zero-shot setting, except for Drop and SQuAD2, which were evaluated in two-shot and one-shot settings respectively.

C CreditDecoding Supplement

In this section, we provide additional details and experiments related to CreditDecoding that were not presented in the main body of the paper.

C.1 Deriving the Minimum Logit Gain

In this subsection, we derive the minimum gain X induced by adding $\log X$ to a token logit, such that the boosted token probability exceeds the confirmation threshold.

Consider a fixed position i at denoising step t with logits $\{l_t^{i,u}\}_{u\in\mathcal{V}}$ and the corresponding softmax distribution

$$p_t^{i,u} = \frac{e^{l_t^{i,u}}}{\sum_{z\in\mathcal{V}} e^{l_t^{i,z}}}. \tag{8}$$

Let $v \in \mathcal{V}$ be the token to be boosted. We apply a logit gain:

$$\hat{l}_t^{i,u} = \begin{cases} l_t^{i,u} + \log X, & u = v, \\ l_t^{i,u}, & u \neq v, \end{cases} \qquad X \geq 1, \tag{9}$$

and define the enhanced distribution by softmax:

$$\hat{p}_t^{i,u} = \frac{e^{\hat{l}_t^{i,u}}}{\sum_{z\in\mathcal{V}} e^{\hat{l}_t^{i,z}}}. \tag{10}$$

Substituting Eq. equation 9 into Eq. equation 10, we obtain

$$\begin{aligned} \hat{p}_t^{i,v} &= \frac{e^{l_t^{i,v}+\log X}}{e^{l_t^{i,v}+\log X} + \sum_{u\neq v} e^{l_t^{i,u}}} \\ &= \frac{X e^{l_t^{i,v}}}{X e^{l_t^{i,v}} + \sum_{u\neq v} e^{l_t^{i,u}}}. \\ &= \frac{X p_t^{i,v}}{(1-p_t^{i,v}) + X p_t^{i,v}}. \end{aligned} \tag{11}$$

To confirm token v under threshold $\tau \in (0,1)$, we require $\hat{p}_t^{i,v} \geq \tau$. By Eq. equation 11,

$$X \geq X_{\min}(p_t^{i,v}, \tau) = \frac{\tau}{1-\tau} \cdot \frac{1-p_t^{i,v}}{p_t^{i,v}}. \tag{12}$$

Apparently, for under-confident tokens (e.g., $p_t^{i,v} \approx 1/|\mathcal{V}|$), the required credit X becomes prohibitively large, validating that naive gain application is risky in early denoising steps with unstable probabilities.

Algorithm 1 CreditDecoding

Input: denoiser f_θ, threshold τ, fusion strength α, decay β, boost exponent γ
Initialize $x_T \leftarrow ([\text{MASK}], \ldots, [\text{MASK}])$
Initialize credit tensor $C \leftarrow \mathbf{0}$ ▷ C is maintained per block
for $t = T, T-1, \ldots, 1$ **do** ▷ Denoising
  for each decoding block $[b_s, b_e)$ **do**
    $x_t^{\text{blk}} \leftarrow x_t[b_s{:}b_e]$
    $m \leftarrow \mathbb{I}\big[x_t^{\text{blk}} = [\text{MASK}]\big]$
    ▷ **Prediction and Greedy selection**
    $\ell \leftarrow f_\theta(x_t)_{b_s:b_e}$
    $p \leftarrow \text{Softmax}(\ell)$
    $(p^{\max}, v^{\max}) \leftarrow \max_{v \in \mathcal{V}} p(\cdot)$
    $\Delta \leftarrow (p^{\max})^\gamma \odot m$
    ▷ **Credit Update**
    $C \leftarrow \beta \cdot C$ ▷ Global decay
    $C \leftarrow C + \text{ScatterAdd}(C,\ v^{\max},\ \Delta)$ ▷ Focused enhancement
    $\hat{\ell} \leftarrow \ell + \alpha \cdot \log(1 + C)$ ▷ Logits fusion
    ▷ **Threshold-based Decoding**
    $\hat{p} \leftarrow \text{Softmax}(\hat{\ell})$
    $(s^{\max},\ \tilde{x}) \leftarrow \max_{v \in \mathcal{V}} \hat{p}(\cdot)$ ▷ Predicted tokens and confidence
    $\text{idx} \leftarrow (s^{\max} \geq \tau) \wedge m$ ▷ Positions to decode
    ▷ **Update block state**
    $x_{t-1}[b_s{:}b_e] \leftarrow \text{where}(\text{idx},\ \tilde{x},\ x_t^{\text{blk}})$
  end for
end for
return x_0

C.2 Algorithm

To accurately illustrate the workflow of the CreditDecoding algorithm, we present its detailed steps in Algorithm 1. Here, T denotes the decoding step, and r,s,t correspond to the mask ratios of the previous, current, and subsequent steps, respectively. Lines 4–12 describe the process of trace credit accumulation, where historical trace credits are decayed by a factor β and the token with the highest confidence is assigned additional trace credit. Lines 13–14 show the application of trace credit, in which past information is integrated into the current step by fusing it with the original logits. Finally, Lines 16–23 represent the mainstream approach to parallel decoding, namely the thresholding method, whose effectiveness has been demonstrated in Fast-dLLM(Wu et al., 2025).

C.3 Ideal Decoding Boundary

In Figure 8, we illustrate the decoding boundaries of three methods, LLaDA, Fast-dLLM, and CreditDecoding, within a single plot. Figure 5 further presents the decoding boundaries (highlighted by red lines) from the perspective of confidence rank, along with an analysis of the ideal decoding boundary. For a more intuitive comparison, the ranges of the plots in Figure 8 are aligned, whereas the

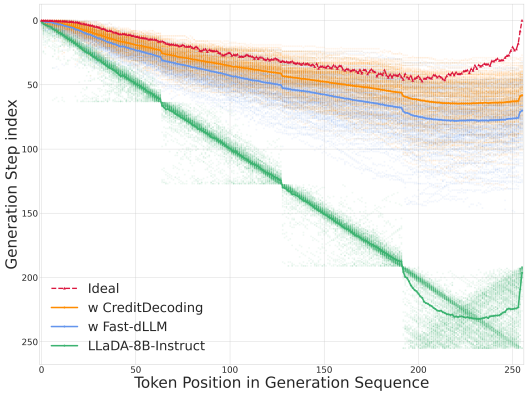

Figure 8: **Decoding Boundary between token stabilization and final decoding.** Evaluated on GSM8K using LLaDA-8B-Instruct, the *red* curve represents the theoretical decoding bound, while others show actual confirming bound. The persistent gap highlights the computational redundancy where correct tokens are repeatedly remasked despite early stabilization.

vertical scales of the three subplots in Figure 5 differ to emphasize the detailed variations introduced by thresholding. The line connecting the first appearance of yellow points, which indicate the initial top-1 confidence, represents the ideal decoding boundary.

It is worth noting that, as shown in Figure 5, different methods yield different ideal decoding boundaries. This variation arises because each method receives distinct inputs at every step, resulting in different confidence distributions. Importantly, stronger models or more effective methods tend to produce an ideal decoding boundary that shifts upward. Our CreditDecoding approach, however, is orthogonal to most existing methods and can further improve their ideal decoding boundaries, bringing the actual decoding boundary closer to the ideal one.

In Figure 9, we visualize the accumulated decoded tokens per step for LLaDA, Fast-dLLM, and CreditDecoding on specific datasets. Two key observations emerge: First, same method speedup varies across datasets. Second, CreditDecoding consistently outperforms Fast-dLLM, especially on SQuAD2.0, where it reduces the decoding steps by an additional 5% step compared to Fast-dLLM's 20% step. As an orthogonal method, CreditDecoding offers greater improvements with higher speedups.

C.4 Block Length Ablation

In the parallel decoding framework of generative models, the choice of generation block length di-

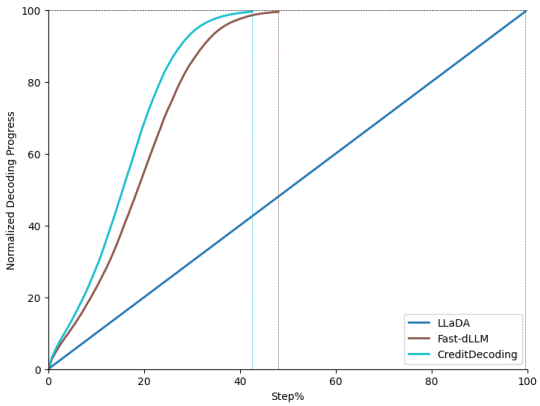

(a) Normalized Decoding Progress on GSM8K

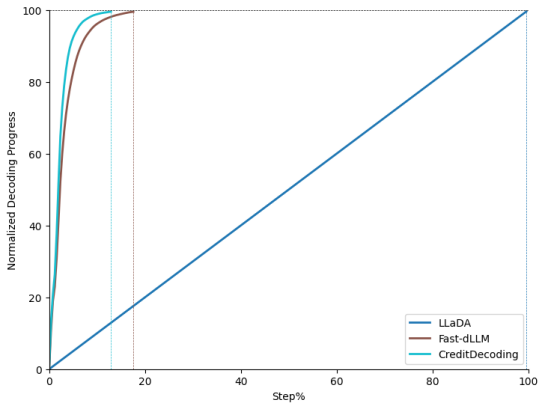

(b) Normalized Decoding Progress on SQuAD2.0

Figure 9: Normalized Decoding Progress **w/o Early Stop** on **GSM8K** and **SQuAD2.0**. We demonstrate the *decoding progress* through visualizing the accumulated number of decoded tokens per step, using **LLaDA-8B-Instruct** with *generation length* $= 256$ and *block size* $= 64$.In order to ensure comparability of the decoding progress, we did not use early stopping. The vertical dashed lines in the figure mark the decoding step at which each method completes, and the ratio of these steps represents the speedup.

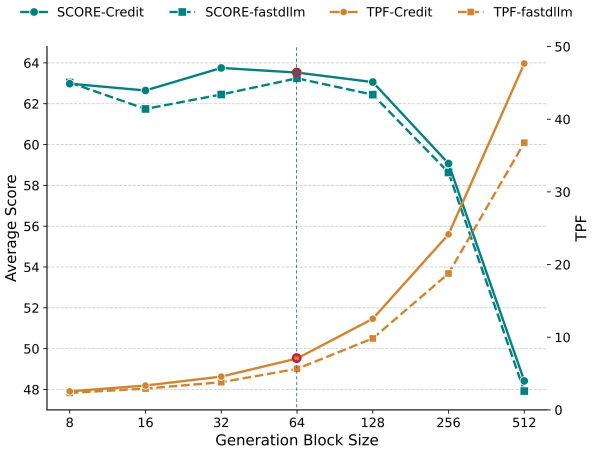

Figure 10: Block Length Abaltion Study

rectly determines the balance between system performance and efficiency. Through block length ablation experiments analyzing Fast-dLLM and CreditDecoding, as shown in Figure 10, it can be observed that when the block length is set to 64, both methods demonstrate relatively superior comprehensive performance. Under this configuration, both CreditDecoding and Fast-dLLM achieve excellent average scores, indicating that this scale fully unleashes the potential of block-level generation mechanisms without significantly sacrificing generation quality. In contrast, smaller block lengths (such as 32) can maintain high performance levels but result in significantly lower decoding speeds, making it difficult to meet the high-throughput requirements of practical deployment. Meanwhile, larger block lengths (such as 256 and above) significantly improve TPF but lead to a sharp performance decline. Therefore, a block length of 64 achieves the optimal balance between maintaining generation performance and achieving parallel acceleration, making it an ideal choice that considers both accuracy and practicality.

Further comparison between CreditDecoding and Fast-dLLM, as illustrated in Figure 10, reveals that CreditDecoding demonstrates greater advantages in overall performance. In terms of performance, CreditDecoding consistently performs on par with or slightly better than Fast-dLLM under medium and small block lengths , reaching its performance peak at a block length of 32, which demonstrates stronger capabilities. Even when both methods experience performance degradation under large block lengths, CreditDecoding still exhibits better error control. Regarding speed, CreditDecoding shows higher TPF across all block length scales, and the performance gap widens as block length increases, reflecting its architectural advantages in parallel scenarios. In summary, CreditDecoding's core value lies in its superior generation performance compared to Fast-dLLM, along with higher overall efficiency. Future work could explore adaptive block sizing or hybrid decoding strategies to dynamically adjust block length and further optimize the balance between performance and speed across different sequence lengths.

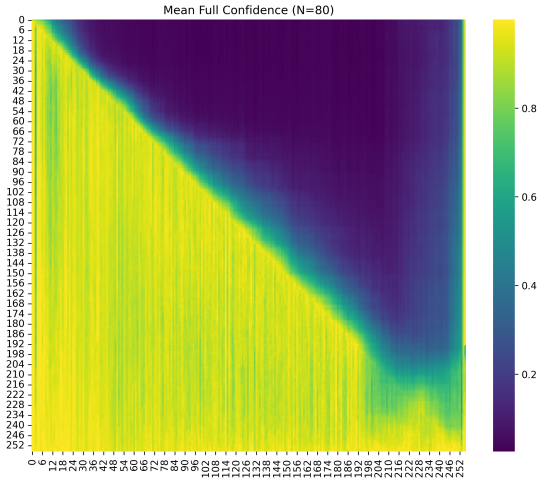

(a) Token Confidence(GSM8K)

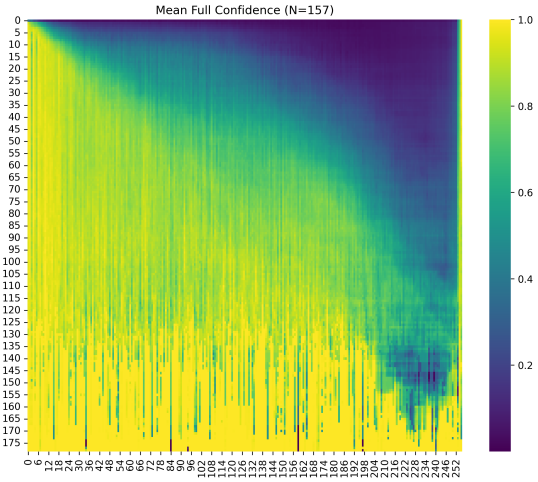

(b) Token Confidence(HumanEval)

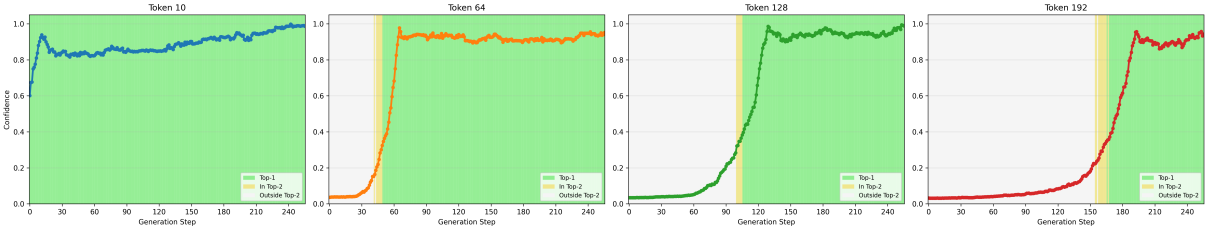

(c) Baseline Confidence Convergence(GSM8K)

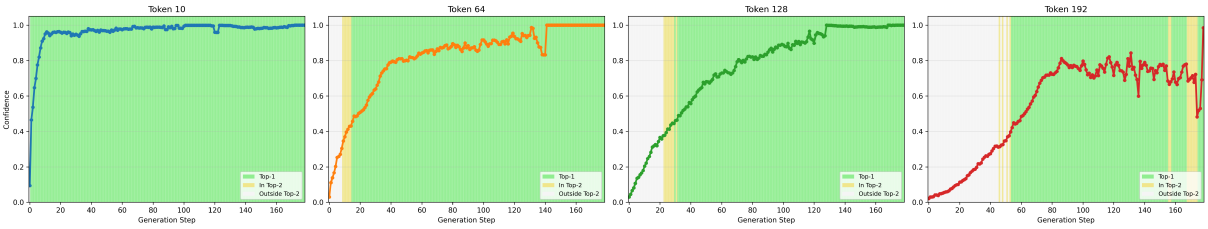

(d) Baseline Confidence Conv.(HumanEval)

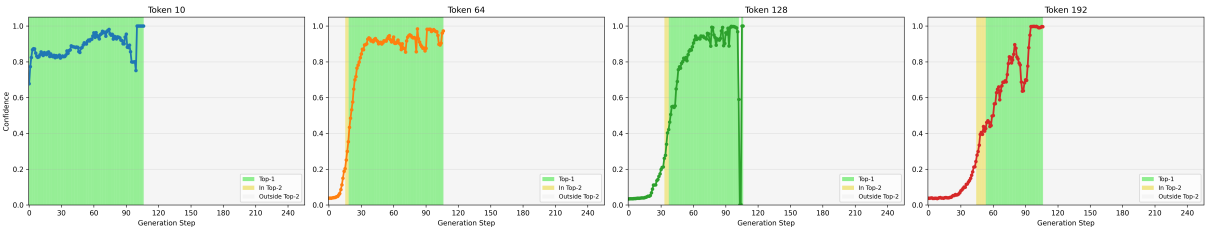

(e) Credit Confidence Conv(GSM8K))

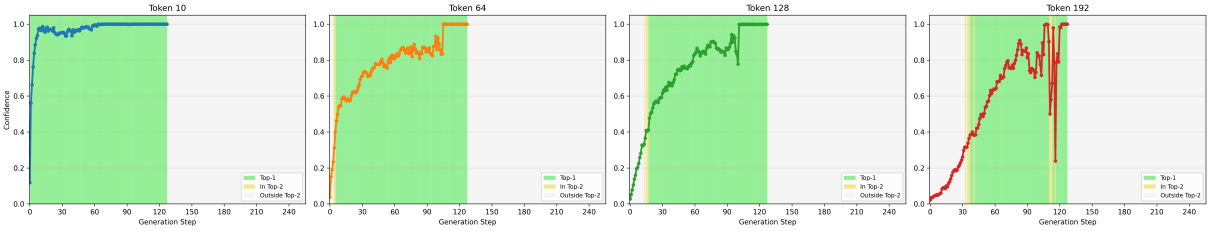

(f) Credit Confidence Conv.(HumanEval)

Figure 11: Token confidence across datasets. Figures (a) and (b) present the average confidence of N tokens at each position during inference. Figures (c)–(f) illustrate the convergence behavior of four representative tokens located at positions 10, 64, 128, and 192, respectively. Results in (a), (c), and (e) are sampled from GSM8K, while those in (b), (d), and (f) are from HumanEval. Panels (c) and (d) show baseline convergence, and (e) and (f) show convergence with CreditDecode.

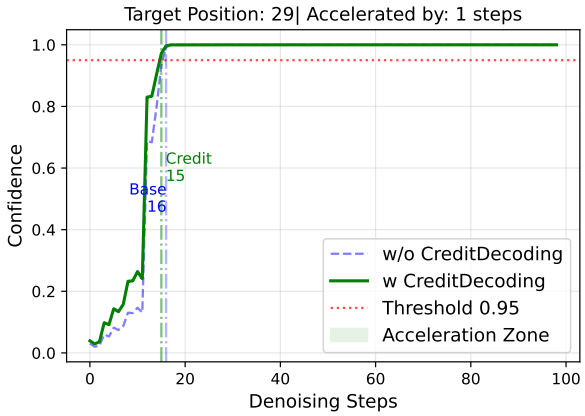

Figure 12: A case study comparing the confidence evolution of a target token under Fast-dLLM and CreditDecoding. It illustrates the direct impact of trace credits on a single token. While this local gain appears minor, it iteratively improves the context for subsequent tokens, which ultimately yields a 21.3% reduction in total inference steps.

C.5 Contextual Cumulative Effect

Notebly, CreditDecoding does not merely accelerate the confirmation of an individual token; by confirming some tokens earlier, it improves the context for subsequent denoising steps and can increase the confidence of other still-masked positions as well. Figure 12 provides a representative example: although CreditDecoding reduces the number of denoising steps, the confidence trajectory of the target token remains largely unchanged, suggesting that the speedup mainly stems from earlier confirmations enabled by improved intermediate context, rather than altering the model's intrinsic predictions.

C.6 Dataset-Dependent Decoding Traces

Further analysis in Figure 11 compares GSM8K and HumanEval. GSM8K requires more context from prior steps, leading to delayed but sharp confidence gains, while HumanEval shows earlier, gradual confidence increases. With CreditDecoding, HumanEval retains its confidence trend while reducing inference steps, whereas GSM8K experiences minor fluctuations that contribute to the performance drop reported in Table 1.

In Figures 11 (c) and (d), we observe the confidence convergence of four specific tokens. On GSM8K, the confidence increase is delayed for tokens later in the sequence, indicating that later tokens rely on earlier tokens to build confidence. Once earlier tokens are confirmed, confidence increases rapidly. On HumanEval, confidence increases earlier in the sequence but at a slower rate.

In Figures 11 (e) and (f), after applying CreditDecoding, we see that for HumanEval, CreditDecoding retains the original confidence trends while reducing the total inference steps, leading to faster inference without loss of accuracy. For GSM8K, early predictions introduce slight confidence fluctuations, contributing to the performance degradation observed in Table 1.

CreditDecoding essentially reduces the inference complexity by leveraging past judgments, improving both accuracy and efficiency. Its goal is to approach the yellow-blue boundary in Figures (a) and (b), representing the theoretical limit of acceleration. As more powerful base models emerge, the acceleration ceiling of CreditDecoding will increase, leading to further efficiency gains in model inference.

Table 4: Orthogonality analysis of CreditDecoding (CD) combined with various optimizations. The baseline setting is **w/o Early Stop**. Values in parenthesis/subscript denote the improvement brought by CD.

Method	TPS	TPF	Score
LLaDA-8B-Instruct			
Standard Inference	7.95	1.00	60.12
+ *CreditDecoding*	$34.90_{+339\%}$	$15.39_{+1439\%}$	$60.73_{+0.61}$
Fast-dLLM (w/o KV)	28.90	12.64	60.11
+ *CreditDecoding*	$34.90_{+21\%}$	$15.39_{+22\%}$	$60.73_{+0.62}$
Fast-dLLM (w/ KV)	39.38	4.42	58.51
+ *CreditDecoding*	$51.40_{+31\%}$	$14.00_{+217\%}$	$58.63_{+0.12}$
Early Stop	9.70	1.00	59.94
+ *CreditDecoding*	$37.33_{+285\%}$	$6.98_{+598\%}$	$60.75_{+0.81}$
Pytorch Compiler	9.03	1.00	60.26
+ *CreditDecoding*	$39.51_{+337\%}$	$15.41_{+1441\%}$	$60.43_{+0.17}$
LLaDA-MoE-Instruct			
Standard Inference	3.53	1.00	62.73
+ *CreditDecoding*	$15.26_{+333\%}$	$14.80_{+1380\%}$	$62.97_{+0.24}$
Fast-dLLM (w/o KV)	13.30	13.08	62.74
+ *CreditDecoding*	$15.26_{+15\%}$	$14.80_{+13\%}$	$62.97_{+0.23}$
FP8 Quantization	2.72	1.00	62.47
+ *CreditDecoding*	$11.87_{+336\%}$	$14.45_{+1345\%}$	$62.58_{+0.11}$
Early Stop	5.11	1.00	62.66
+ *CreditDecoding*	$16.99_{+233\%}$	$4.77_{+377\%}$	$62.92_{+0.26}$
Pytorch Compiler	2.42	1.00	63.29
+ *CreditDecoding*	$10.72_{+343\%}$	$14.88_{+1388\%}$	$62.99_{-0.3}$

C.7 Orthogonality

In Section 5.6, we demonstrate the orthogonality and compatibility of CreditDecoding through experiments combining it with several acceleration techniques. Results show that CreditDecoding consistently improves both speed and performance

Table 5: Main benchmark results **w/ Early Stop** across eight datasets on **LLaDA-8B-Instruct** (Gen Length=256, Block Size=64). Cells show **Score** (top, relative to LLaDA) and **TPF** (bottom, improvement over Fast-dLLM).

Benchmark (Score / TPF)	Fast-dLLM	CD	CD†
MMLU	62.43$_{-0.03}$ 2.86	**63.78**$_{+1.32}$ **4.57**$_{+56\%}$	63.66$_{+1.20}$ 3.38$_{+18\%}$
SQuAD2.0	91.43$_{+0.00}$ 13.55	**91.71**$_{+0.28}$ **16.84**$_{+24\%}$	91.48$_{+0.05}$ 15.07$_{+11\%}$
DROP	82.74$_{-0.12}$ 2.93	**82.78**$_{-0.08}$ **3.79**$_{+29\%}$	82.70$_{-0.16}$ 3.15$_{+8\%}$
KorBench	33.20$_{+0.08}$ 3.72	**35.04**$_{+1.92}$ **5.03**$_{+35\%}$	33.92$_{+0.80}$ 4.43$_{+19\%}$
HumanEval	34.15$_{-0.61}$ 3.82	36.59$_{+1.83}$ **4.69**$_{+23\%}$	**37.80**$_{+3.04}$ 4.18$_{+9\%}$
LCB	8.15$_{+0.00}$ 1.93	7.54$_{-0.61}$ **2.17**$_{+12\%}$	7.71$_{-0.44}$ 2.00$_{+4\%}$
GSM8K	**78.47**$_{+0.53}$ 3.22	77.18$_{-0.76}$ **3.87**$_{+20\%}$	77.48$_{-0.46}$ 3.39$_{+5\%}$
Math	37.04$_{-0.26}$ 2.42	**37.24**$_{-0.06}$ **2.84**$_{+17\%}$	37.18$_{-0.12}$ 2.55$_{+5\%}$
Average	53.45$_{-0.05}$ 4.31	53.98$_{+0.48}$ **5.48**$_{+27\%}$	**53.99**$_{+0.49}$ 4.77$_{+11\%}$

Table 6: Main benchmark results **w/ Early Stop** across eight datasets on **LLaDA-MoE-Instruct**. (Gen Length=256, Block Size=64). Cells show **Score** (top, relative to LLaDA-MoE) and **TPF** (bottom, improvement over Fast-dLLM).

Benchmark (Score / TPF)	Fast-dLLM	CD	CD†
MMLU	64.08$_{+0.00}$ 2.16	**64.21**$_{+0.13}$ **2.46**$_{+14\%}$	63.94$_{-0.14}$ 2.33$_{+8\%}$
SQuAD2.0	86.88$_{+0.00}$ 7.09	87.27$_{+0.39}$ **9.64**$_{+36\%}$	**87.35**$_{+0.47}$ 8.41$_{+19\%}$
DROP	**80.16**$_{+0.00}$ 2.73	79.72$_{-0.44}$ **3.28**$_{+20\%}$	79.87$_{-0.29}$ 2.92$_{+7\%}$
KorBench	**36.88**$_{+0.16}$ 2.36	36.48$_{-0.24}$ **3.28**$_{+38\%}$	36.64$_{-0.08}$ 2.73$_{+16\%}$
HumanEval	51.22$_{+0.00}$ 4.97	51.22$_{+0.00}$ **6.00**$_{+21\%}$	**53.05**$_{+1.83}$ 5.45$_{+10\%}$
LCB	14.04$_{+0.16}$ 2.43	14.37$_{+0.49}$ **2.81**$_{+16\%}$	**14.65**$_{+0.77}$ 2.55$_{+5\%}$
GSM8K	74.45$_{+0.08}$ 2.28	**74.98**$_{+0.61}$ **2.68**$_{+18\%}$	74.37$_{+0.00}$ 2.42$_{+6\%}$
Math	35.84$_{-0.18}$ 2.35	**36.28**$_{+0.26}$ **2.71**$_{+15\%}$	36.26$_{+0.24}$ 2.48$_{+6\%}$
Average	55.44$_{+0.02}$ 3.30	55.57$_{+0.15}$ **4.11**$_{+25\%}$	**55.77**$_{+0.35}$ 3.66$_{+11\%}$

across all tested methods.

In this section, we provide brief introductions to the acceleration methods discussed in Section 5.6 and include additional TPS results to better illustrate CreditDecoding's effectiveness, particularly on system-level accelerations that mainly improve TPS. We also extend our orthogonality analysis to LLaDA-MoE, with detailed results presented below.

We evaluate its orthogonality on four representative acceleration techniques, as illustrated in Figure 1.

Early Stop: Early Stop terminates decoding when the current token is <EOS> and all previous tokens are finalized, effectively reducing redundant generation and improving decoding efficiency.

Fast-dLLM (Wu et al., 2025): A state-of-the-art acceleration method consisting of threshold-based parallel decoding and KV Cache. Since the KV Cache significantly increases TPS at the cost of performance, we mainly compare with Fast-dLLM (w/o KV).

PyTorch Compiler (Jain et al., 2023): PyTorch Compiler leverages graph-level optimizations for runtime acceleration without altering decoding behavior.For MoE architecture, compiler can fuse MoE kernel which highly accelerate the inference process.

FP8 Quantization (Kwon et al., 2023): FP8 quantization is a technique that reduces the precision of floating-point numbers to 8-bit, aiming to accelerate deep learning models by lowering storage and computation costs while maintaining sufficient accuracy.

Table 4 presents detailed results corresponding to Figure 1, including TPS comparisons and reports results under the same settings on LLaDA-MoE, further including FP8 quantization.

C.8 Full-Distribution Trace Credit

In Sec. 4.2, trace credit is accumulated only on the decoded (top-1) token at each step. This focused strategy concentrates reinforcement and yields stronger acceleration, but it may ignore useful probability mass on other plausible candidates.

To examine the generality of credit accumulation beyond the top-1 hypothesis, we also consider a full-distribution variant that updates all tokens:

$$C_t^{i,v} = \beta C_{t+1}^{i,v} + (p_t^{i,v})^{\gamma}, \qquad \forall v \in \mathcal{V}. \tag{13}$$

By aggregating historical evidence over the entire predictive distribution, this variant becomes less sensitive to transient noise and confidence oscillation. Intuitively, it can achieve slightly higher accu-

racy but weaker acceleration compared to the standard version, forming a more conservative trade-off option.

We evaluate this full-distribution variant (denoted as **CD**†) alongside the standard CreditDecoding (**CD**). Tables 5 and 6 report results on LLaDA-8B-Instruct and LLaDA-MoE-Instruct across eight benchmarks.

Overall, **CD**† delivers slightly larger accuracy improvements than **CD** (+0.49 vs. +0.48 on LLaDA-8B and +0.35 vs. +0.15 on LLaDA-MoE), while incurring around 10% lower speedup due to its weaker reinforcement strength. Nevertheless, **CD**† still achieves substantial acceleration, showing that aggregating credit over the full predictive distribution remains effective relative to the baseline.

These results provide two important insights. First, the comparable (and sometimes higher) accuracy of **CD**† indicates that credit accumulation is fundamentally general and does not rely on reinforcing only the final decoded token. Second, **CD** achieves stronger acceleration, indicating that assigning credit only to the top-1 predicted token is sufficient. Since the decoded token typically remains the top-1 prediction for several consecutive steps, this *focused reinforcement* is both stable and computationally efficient.

Unlike **CD**, the full-distribution variant requires maintaining credits for every token in the vocabulary and updating them at each denoising step, which introduces non-trivial memory and computational overhead. Therefore, **CD** provides a better efficiency–accuracy trade-off and remains the recommended default in practice.